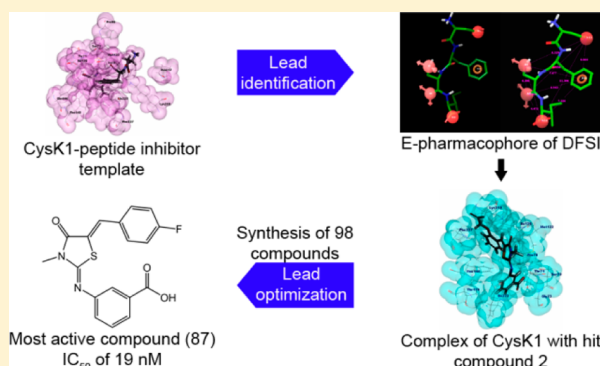


Structure-Guided Design of Novel Thiazolidine Inhibitors of O-Acetyl Serine Sulfhydrylase from *Mycobacterium tuberculosis*Ömer Poyraz,^{†,||} Variam Ullas Jeankumar,^{‡,||} Shalini Saxena,[‡] Robert Schnell,[†] Martin Haraldsson,[†] Perumal Yogeewari,[‡] Dharmarajan Sriram,^{*,‡} and Gunter Schneider^{*,†}[†]Division of Molecular Structural Biology, Department of Medical Biochemistry & Biophysics, Karolinska Institutet, S-171 77 Stockholm, Sweden[‡]Drug Discovery Research Laboratory, Department of Pharmacy, Birla Institute of Technology & Science—Pilani, Hyderabad Campus, Shameerpet, R.R. District, Hyderabad-500078, Andhra Pradesh, India^{*}Chemical Biology Consortium Sweden, Science for Life Laboratory, Department of Medical Biochemistry & Biophysics, Karolinska Institutet, S-171 77 Stockholm, Sweden

S Supporting Information

ABSTRACT: The cysteine biosynthetic pathway is absent in humans but essential in microbial pathogens, suggesting that it provides potential targets for the development of novel antibacterial compounds. CysK1 is a pyridoxalphosphate-dependent O-acetyl sulfhydrylase, which catalyzes the formation of L-cysteine from O-acetyl serine and hydrogen sulfide. Here we report nanomolar thiazolidine inhibitors of *Mycobacterium tuberculosis* CysK1 developed by rational inhibitor design. The thiazolidine compounds were discovered using the crystal structure of a CysK1–peptide inhibitor complex as template. Pharmacophore modeling and subsequent in vitro screening resulted in an initial hit compound 2 (IC₅₀ of 103.8 nM), which was subsequently optimized by a combination of protein crystallography, modeling, and synthetic chemistry. Hit expansion of 2 by chemical synthesis led to improved thiazolidine inhibitors with an IC₅₀ value of 19 nM for the best compound, a 150-fold higher potency than the natural peptide inhibitor (IC₅₀ 2.9 μM).



■ INTRODUCTION

Mycobacterium tuberculosis, the causative agent of tuberculosis (TB), is one of the most devastating human pathogens worldwide. Treatment of this disease is becoming increasingly complicated due to the alarming occurrence of multidrug-resistant (MDR) or extremely drug-resistant (XDR) strains of *M. tuberculosis*.^{1,2} Further complications arise from the life cycle of this bacterium, resulting in approximately one-third of the world's population carrying *M. tuberculosis* as latent infection, which is difficult to treat with currently available antibiotics. Latent TB is characterized by dormant bacteria with low metabolic activity that can survive and replicate in macrophages for years.³ The environment of dormant *M. tuberculosis* in infected macrophages of the host is characterized by oxygen depletion, nutrient depletion, and oxidative stress.⁴ To inactivate damaging reactive oxygen species generated by macrophages and hence to maintain redox homeostasis, *M. tuberculosis* uses mycothiol as principal low-molecular-weight antioxidant. This metabolite is present in millimolar concentration in the cytoplasm and is derived from L-cysteine.⁵ Genes involved in the sulfate reduction pathway and cysteine biosynthesis have been found to be up-regulated in different latency models using nutrient or oxygen depletion^{6–8} or

nitrosative stress.⁹ In view of these findings, enzymes involved in sulfur metabolism and cysteine biosynthesis have been proposed as potential targets for the development of novel antimycobacterial compounds.^{10,11}

The classical CysK1 dependent pathway to produce cysteine in *M. tuberculosis* uses hydrogen sulfide as sulfur source, which is derived from the APS–PAPS pathway.¹² CysK1 from *M. tuberculosis* binds specifically to a four residue long peptide derived from the C-terminus of the serine acetyl transferase CysE. This tetrapeptide, with the amino acid sequence DFSI (1, Figure 1), binds in the active site cleft of the enzyme and is a competitive inhibitor of CysK1 with a *K_i* of 5 μM.¹² Previously, we reported the identification of novel inhibitors of CysK1 from *M. tuberculosis* based on virtual high-throughput screening.¹³ In the present study, we utilized the crystal structure of the CysK1–DFSI complex as template in energy-based pharmacophore (e-pharmacophore) modeling and in silico docking to identify nonpeptidic compounds as putative active site ligands. One thiazolidine compound, 3-({5-[2-(carboxymethoxy)benzylidene]-3-methyl-4-oxo-1,3-thiazolidin-

Received: May 13, 2013

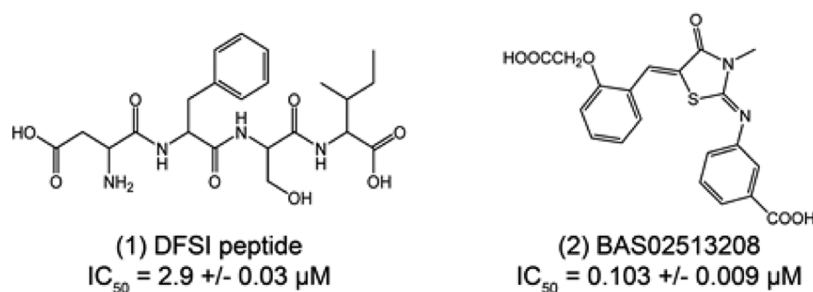


Figure 1. Structure of the inhibitory peptide DFSI used as template (left) and structure of the best hit 2, 3-({5-[2-(carboxymethoxy)benzylidene]-3-methyl-4-oxo-1,3-thiazolidin-2-ylidene}amino)benzoic acid (right), from e-pharmacophore modeling used for further inhibitor improvement and further SAR studies.

2-ylidene}amino)benzoic acid (2), within this set was identified as a strong inhibitor of CysK1 with an IC_{50} in the nM range (Figure 1) and chosen for improvement and further SAR studies.

RESULTS AND DISCUSSION

In the first step, the e-pharmacophore approach, which combines aspects of structure-based and ligand-based techniques, was explored to identify small molecules that bind to the active site of CysK1 using the crystal structure of the CysK1–peptide inhibitor complex (PDB entry 2Q3C)¹² as template. The pharmacophore hypotheses based on mapping of the energetic terms from the extra precision Glide scoring function (Glide XP) (Glide, version 5.7, Schrödinger, LLC, New York, NY, 2011)^{14–16} onto atom centers was employed to derive pharmacophore sites. These were based on the structural and energy information between the protein and the ligand using phase (Phase, v3.3, Schrödinger, LLC, New York, NY). The maximum number of pharmacophore sites derived for the DFSI peptide was five with two acceptors (A), two negative ionizable groups (N), and one aromatic ring (A) (Figure 2). The five-point e-pharmacophore was then utilized for the virtual screening of a commercial database (Asinex) using a protocol described in more detail in the Experimental Section of the Supporting Information and summarized in Figure 2.

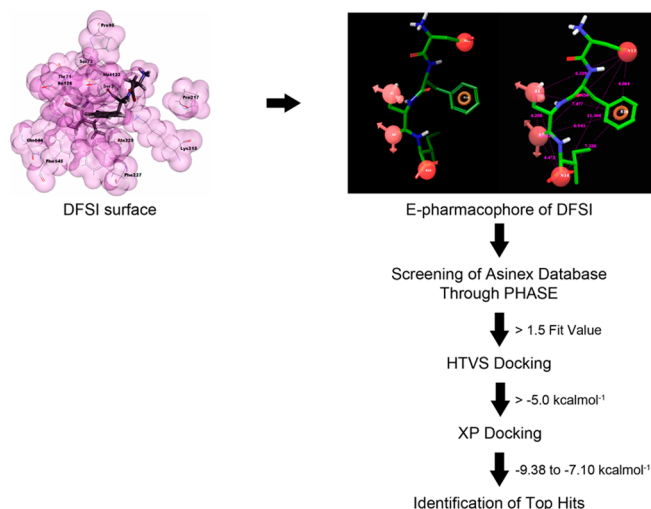


Figure 2. Workflow for the identification of initial hits of *Mycobacterium tuberculosis* CysK1 inhibitors by e-pharmacophore modeling and in silico docking. The protocol started with the structure of the enzyme with the bound peptide inhibitor, DFSI.

Compounds retrieved by the e-pharmacophore model using phase with a fit value above 1.5 were regarded as potential hits and were carried forward for high-throughput virtual screening. Top compounds from this screen resulting in a score of ≥ -5.0 kcal mol⁻¹ and docked with three or more hydrogen bonds were subjected to another round of docking by Glide XP. The GlideXP combines accurate, physics-based scoring terms and thorough sampling, and the results gave scores ranging from -9.38 to -7.10 kcal mol⁻¹. Final shortlisting of possible hit compounds was based on visual inspection of the important amino acid residues in the active site cleft involved in binding that included hydrogen bonds to Thr71, Gln144, Ser72, and Lys215 and hydrophobic interactions with Phe145. The selected hits retrieved from the Asinex database were experimentally screened at a compound concentration of 2 mM against *M. tuberculosis* CysK1 using an assay based on the spectrophotometric determination of the reaction product L-cysteine adapted to 96-well plate format described previously.¹² Twenty-eight compounds displayed >80% inhibition, and these were rescreened at 100 μM inhibitor concentration. Seven out of those showed >80% inhibition under these conditions (Supporting Information Figure 2), with the thiazolidine compound 2 (Figure 1) being the most potent inhibitor with an IC_{50} of 103 nM.

To provide a structural basis for further inhibitor improvement, we determined the crystal structure of the complex of CysK1 with 2 to a resolution of 2.0 Å (Figure 3 and Supporting Information Table 1). The overall structure of the enzyme in the complex is very similar to the structure in the enzyme–peptide complex (root-mean-square deviation value after structural superposition of 0.3 Å for 300 equivalent α -atoms). The electron density map showed that 2 was bound in the active site cleft (Figure 3A). The experimentally observed binding mode of the ligand agrees well with the predicted binding from the e-pharmacophore modeling, with an rmsd of 0.8 Å after superimposition. However, there are significant differences of 2 to the DFSI binding mode (Figure 3B). While the DFSI peptide extends from the active site to the protein surface, 2 is, with the exception of the 2-carboxymethylether headgroup, bound entirely in the cleft between the two domains. The benzoic acid is buried in the interior of the active site with its carboxyl group occupying the same position as the carboxyl groups of the C-terminal isoleucine residue of the DFSI peptide and aminoacrylate reaction intermediate.¹² One of the carboxyl oxygen atoms of the benzoic acid moiety interacts with the backbone amide nitrogen atom of Ser72 from the conserved ⁷¹TSTGNT⁷⁵ serine loop (Figure 4). The second oxygen atom is within hydrogen bond distance to the side chains of Thr71 and Gln144 and a water molecule. The phenyl

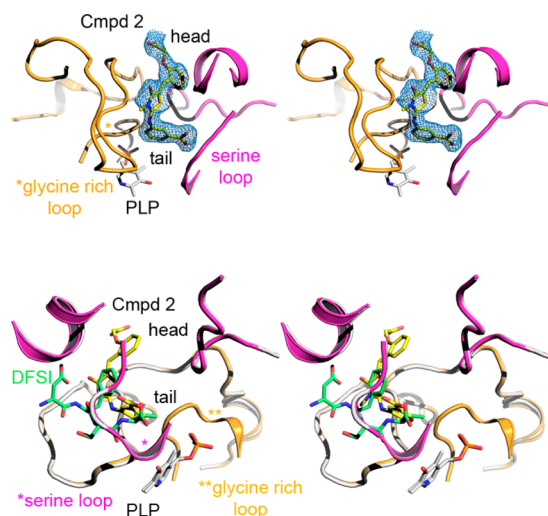


Figure 3. (Upper panel) Stereo view of the unbiased $F_o - F_c$ difference electron density map at 3.0σ for the bound ligand **2**. The electron density map is shown in blue, with the bound ligand shown as a stick model. Loops constituting the active site cleft are colored in magenta (N-terminal domain) and orange (C-terminal domain). (Lower panel) Superposition of the peptide inhibitor DFSI (green) with the thiazolidine compound **2** (yellow) bound to the active site of CysK1.

ring occupies the same position as the isoleucine side chain of the peptide and packs against Phe145, Gly178, Gly222, and Ala225. These interactions directly match those observed for the DFSI C-terminal isoleucine residue. The thiazolidine core mimics the phenyl ring of the DFSI peptide and occupies an equivalent position within the hydrophobic pocket formed by Met122, Phe145, Ala225, and Phe227. Its ring plane is almost perpendicular to that of the benzoic acid moiety. The keto group in ring position 2 points toward the protein surface and forms hydrogen bonds with the side chain of Lys215 and a water molecule. Distinct to the DFSI peptide, whose N-terminal aspartic acid residue extends to the protein surface, the benzylidene moiety of **2** occupies a hydrophobic pocket inside the cleft (Figures 3 and 4). This pocket is located close to the protein surface and is surrounded by Pro70, Ile126, Phe145, and Phe227. Finally, the 2-carboxymethoxy substitution in ring position 10 extends toward the solvent and neither the ether oxygen atom nor the carboxyl headgroup are involved in any hydrogen bonding. In addition the structure of the CysK1–**2** complex revealed two pockets adjacent to the N3-methyl group

of the thiazolidine ring and the *para*-position of the benzylidene moiety, respectively, that potentially could be explored for modifications of the inhibitor scaffold (Figure 4B).

The promising results of the virtual screening hits and the 2.0 Å structure of the enzyme–hit complex encouraged us to design a library with the goal of obtaining a lead series with tractable SAR and potencies better than the identified initial screening hits. Investigation of thiazolidinone and thiazolidinedione pharmacophores has recently generated significant interest from a medicinal chemistry point of view,^{17–20} and their synthesis has been well explored in the literature.^{21,22} The synthetic pathway used to achieve the lead modifications is delineated in Scheme 1 and described in more detail in the Supporting Information.

On the basis of the input from protein–ligand interactions observed in the structure of CysK1 with **2**, the following modifications (and combinations thereof) were explored in a first ligand expansion step: (i) extending the alkyl chain attached to the nitrogen (N-3) of the thiazolidinone core (–N-methyl (R_1)) with an ethyl, propyl, isopropyl, allyl, or butyl group and also modifying the OCH_2COOH (R_3) substitution at the *ortho* position of the phenyl ring in the hit molecule with –OH, $\text{OCH}_2\text{COOCH}_3$ (**9–17**) and (ii) shifting these groups from the *ortho* to the *para* position (**18–48**) to identify the ideal sites for introducing chemical diversity and to have a clearer understanding of the role of these substituents as determinants of inhibitory potency.

A library of 40 derivatives (sublibrary 1) was synthesized (compounds **9–48**, Tables 1 and 2) and evaluated for their ability to inhibit CysK1 as steps toward the derivation of structure–activity relationships (SAR) and hit optimization. The inhibition of *M. tuberculosis* CysK1 for compounds **9–17** (Table 1) at 500 nM was not encouraging because all substitutions led to less potent molecules compared to the initial hit **2**. However, substitutions at the *para*-position of the benzylidene ring highlighted this position as an important determinant of inhibitory potency (**18–48**) (Table 2). Whereas the analogues of $\text{OCH}_2\text{COOH}/\text{OCH}_2\text{COOCH}_3$ modifications in the *para*-position showed little inhibition of CysK1, the corresponding hydroxy derivatives (**18**, **19**, **22**, **25**, **28**, and **31**) resulted in molecules with similar or improved IC_{50} values compared to **2**. Among these derivatives (Table 2), the order of activity with respect to the N-substitution (R_1) was methyl > propyl > ethyl > allyl > isopropyl > butyl substitution, i.e., suggests a preference for a short alkyl side chain at this position. Finally, replacement of the carboxylic acid group in the secondary phenyl ring by an acetyl moiety (**34–48**) was

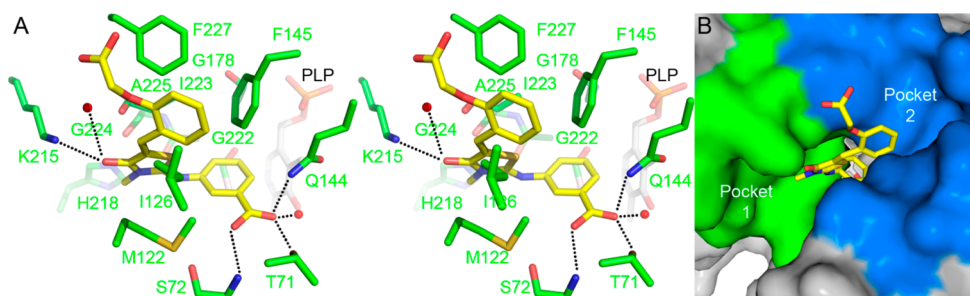
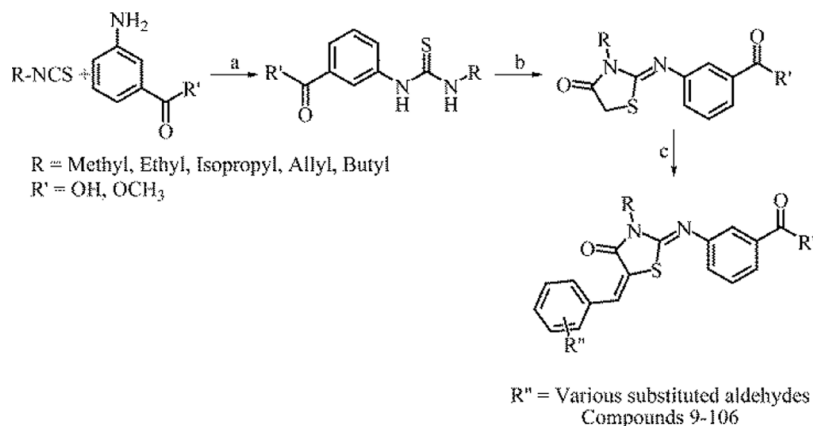


Figure 4. (A) Stereo view of the active site in the CysK1–**2** complex. The amino acid side chains (green) and the bound thiazolidine inhibitor **2** (yellow) are shown as sticks and water molecules are shown as red spheres. Hydrogen bonds are indicated by dashed lines. (B) Surface representation of the ligand binding site in the CysK1–**2** complex highlighting pocket 1 (green) proximal to the thiazolidine core and pocket 2 (blue) adjacent to the benzylidene moiety of the ligand.

Scheme 1. Synthetic Protocol to Thiazolidine Analogues^a

^a (a) (C₂H₅)₃N, CHCl₃, 0 °C to rt, 12 h; (b) BrCH₂COOH, CH₃COONa, C₂H₅OH, reflux; (c) substituted aldehydes, piperidine, ethanol reflux.

Table 1. Activities of Synthesized Compounds (9–17)

compd	R ₁	R ₂	% inhibition at 500 nM
9	methyl	OH	62.7 ± 9.3
10	methyl	OCH ₂ C(=O)OCH ₃	56.3 ± 4.5
11	ethyl	OH	53.2 ± 6.3
12	ethyl	OCH ₂ C(=O)OCH ₃	31.0 ± 10.9
13	ethyl	OCH ₂ C(=O)OH	15.9 ± 7.7
14	allyl	OCH ₂ C(=O)OCH ₃	38.6 ± 7.8
15	allyl	OCH ₂ C(=O)OH	25.4 ± 5.6
16	isopropyl	OCH ₂ C(=O)OCH ₃	55.7 ± 9.0
17	isopropyl	OCH ₂ C(=O)OH	18.5 ± 7.0

detrimental to bioactivity as it resulted in inactive molecules (Table 2). This observation highlights the importance of a carboxyl group at this position and is consistent with the tight interactions through hydrogen bonding observed in the complexes of CysK1 with the reaction intermediate, the peptide inhibitor,¹² the initial hit **2** (Figure 2A) as well as CysK–peptide complexes from other species.^{23–25}

On the basis of these observations, a new sublibrary was designed and synthesized that incorporated the importance of a small alkyl chain at the R₁ position and further explored pocket 2 by a series of substitutions on the phenyl ring. This sublibrary of 60 molecules (**49–106**) was designed and synthesized by modifying various parts of the ligand as shown in Tables 3 and 4 using commercially available substituted benzaldehydes and heterocyclic aldehydes and employing a similar protocol as outlined in Scheme 1. In vitro characterization of these compounds showed that for substitutions at the C-2 position only the methoxy derivative with *N*-methyl substitution **67** gave a potent inhibitor (IC₅₀ 160 nM), whereas substitutions with bromo, chloro, *O*-benzyl, or methyl groups showed significantly less inhibitory activity. At the C-3 position trifluoromethyl and methyl substitutions were studied (**59, 60, 77, 78**) and found to be much less active than the parent compound **2**. Substitutions at the C-4 position resulted in several strongly inhibitory


molecules, with the order of activity fluoro (**87**) > *O*-benzyl (**57**) > *O*-methyl (**51**) > *N,N*-dimethylamino (**93**). Other substitutions like bromo, chloro, isopropyl, nitro, or methyl were less active as inhibitors of CysK1.

Multiple substitutions were also studied including 2,4-dichloro (**63, 64**), 3,4-dichloro (**89, 90**), 3,4-dimethoxy (**83, 84**), 3-methoxy, 4-hydroxy (**81, 82**), and 3,4,5-trimethoxy (**95, 96**) with *N*-methyl or ethyl groups. Among these, 3-methoxy, 2-hydroxy (**81**), 3,4-dimethoxy (**83, 84**), and 3,4,4-trimethoxy (**95**) analogues were found to be very active and their IC₅₀ values were determined (Table 3). Efforts were also made to replace the primary benzyl ring by heteroaryl ring systems, and 10 compounds were synthesized (Table 4). Replacement of the benzyl ring by furan (**97, 98**), pyrrole (**99, 100**), pyridine (**101, 102**), 4-trifluoromethyl, 3-pyridyl (**103, 104**), or indole (**105, 106**) moieties resulted in significant reduction in activity, compared to the best inhibitors from the previous modification step, thus emphasizing a favorably substituted benzyl ring as the primary aryl ring. Among the thiazolidine analogues studied in this work, the 4-fluoro derivative (**87**) emerged as the most potent analogue, with an IC₅₀ of 19 nM, five times more active than the initial hit compound (**2**) and 150 times more potent than the natural peptide DFSI (**1**), the starting point of the inhibitor design in this study.

Overall, the SAR exploring pocket 2 adjacent to the benzylidene ring agreed well with the crystal structure of the complex of CysK1 with **2**. Modeling of the substitutions at the *p*-position of the benzylidene ring of **2**, which led to the best inhibitors, suggests that, in particular, interactions with side chains of residues Pro70, Ile126, Ala129, Val141, and Gln143 could contribute to the increase in binding strength. Substitutions at the N atom of the thiazolidine ring did, however, contrary to expectations, not lead to significant increases in inhibitory activity.

Efforts to obtain well-diffracting crystals of CysK1 with the most potent inhibitors were not successful. For compound **22**, we obtained crystals of the enzyme–ligand complex that however only diffracted to 3.8 Å resolution. The electron density map revealed binding of the inhibitor in the active site cleft of CysK1, but the limited resolution did not allow an unambiguous fit of the inhibitor molecule to the density map. As an alternative method to ascertain that the inhibitors bind in the active site cleft adjacent to the PLP cofactor, we employed a fluorescence-based method whereby the change in PLP

Table 2. Activities of Synthesized Compounds (18–48)



compd	R ₁	R ₂	% inhibition at 500 nM	IC ₅₀ (nM)	compd	R ₁	R ₂	% inhibition at 500 nM	IC ₅₀ (nM)
18	methyl	OH	92.6 ± 0.9	62.6 ± 12.5	34	ethyl	OH	3.4 ± 9.4	nd
19	ethyl	OH	90.2 ± 3.3	101.4 ± 6.7	35	ethyl	OCH ₂ C(=O)OCH ₃	8.2 ± 5.1	nd
20	ethyl	OCH ₂ C(=O)OCH ₃	9.9 ± 8.6	nd	36	ethyl	OCH ₂ C(=O)OH	10.0 ± 1.5	nd
21	ethyl	OCH ₂ C(=O)OH	36.9 ± 7.0	nd	37	propyl	OH	10.7 ± 9.4	nd
22	propyl	OH	95.1 ± 15.5	95.1 ± 15.5	38	propyl	OCH ₂ C(=O)OCH ₃	0.0 ± 3.2	nd
23	propyl	OCH ₂ C(=O)OCH ₃	0 ± 7.7	nd	39	propyl	OCH ₂ C(=O)OH	0.0 ± 8.1	nd
24	propyl	OCH ₂ C(=O)OH	0 ± 5.6	nd	40	allyl	OH	28.9 ± 5.0	nd
25	allyl	OH	92.3 ± 0.9	110.4 ± 24.8	41	allyl	OCH ₂ C(=O)OCH ₃	10.9 ± 3.7	nd
26	allyl	OCH ₂ C(=O)OCH ₃	19.9 ± 9.7	nd	42	allyl	OCH ₂ C(=O)OH	0.0 ± 8.3	nd
27	allyl	OCH ₂ C(=O)OH	1.4 ± 8.6	nd	43	isopropyl	OH	8.2 ± 5.0	nd
28	isopropyl	OH	90.3 ± 0.5	140.6 ± 13.5	44	isopropyl	OCH ₂ C(=O)OCH ₃	7.4 ± 6.5	nd
29	isopropyl	OCH ₂ C(=O)OCH ₃	0 ± 4.7	nd	45	isopropyl	OCH ₂ C(=O)OH	10.2 ± 8.4	nd
30	isopropyl	OCH ₂ C(=O)OH	12.6 ± 6.6	nd	46	butyl	OH	25.1 ± 4.7	nd
31	butyl	OH	78.5 ± 1.5	nd	47	butyl	OCH ₂ C(=O)OCH ₃	0.0 ± 5.5	nd
32	butyl	OCH ₂ C(=O)OCH ₃	16.4 ± 14.0	nd	48	butyl	OCH ₂ C(=O)OH	24.1 ± 2.1	nd
33	butyl	OCH ₂ C(=O)OH	0 ± 8.6	nd					

fluorescence in response to ligand binding is monitored.²⁶ The peptide inhibitor DFSI (1) and inhibitor 2 were used as positive controls as their binding in the proximity of the cofactor was verified by crystal structure analysis. The tested compounds 18, 19, 22, 25, 28, 51, and 57 showed the expected spectral changes in PLP fluorescence as the control consistent with binding of these inhibitors in the active site cleft of CysK1 (Supporting Information Figure 2).

CONCLUSIONS

Previous efforts to develop inhibitors against CysK1 from pathogenic organisms were directed toward improvements of natural peptide inhibitors.^{25,27} Given the unfavorable drug-like properties of peptides, alternative approaches also involved virtual screening^{13,28} and chemical synthesis²⁹ to identify nonpeptidic inhibitors of CysK. These efforts led to small-molecule inhibitors of moderate potency, with IC₅₀ or K_D values in the low μM range. In this study, a combination of ligand-based and structure-based e-pharmacophore modeling has been employed to identify structurally diverse small-molecule ligands of *M. tuberculosis* CysK1 based on the crystal structure of the enzyme with a peptide inhibitor. The thiazolidine scaffold 2 was identified as a potent inhibitor of CysK1 with an IC₅₀ of 103 nM. We determined the crystal structure of the complex of the enzyme with this inhibitor, the first CysK1–nonpeptide inhibitor. The structure revealed hitherto unknown binding pockets and inhibitor binding modes distinct from the peptide binding sites which could be exploited successfully in inhibitor development. Our initial SAR data validated the presence of the carboxyl group of the secondary phenyl ring of the scaffold as essential for strong binding of the inhibitor, consistent with previous structural data.^{12,23–25} Further the *para*-position of the benzylidene group was sensitive to changes and crucial for CysK1 inhibition. A

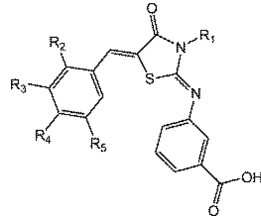
comprehensive SAR was obtained by synthesizing a library of 98 compounds to understand the importance of substitutions in the phenyl ring system and the nitrogen of the thiazolidine nucleus. These findings were used to develop inhibitor 87 (IC₅₀ 19 nM), the most potent CysK1 inhibitor described so far, with a 150 times higher potency than the original DFSI tetrapeptide (IC₅₀ 2.9 μM). This inhibitor, as well as other compounds in this series, have favorable log *P* values (2.7–5.3), and the ADME values predicted using the Schrödinger software are in acceptable ranges. The study provides the basis for further chemical optimization of these potent thiazolidine inhibitors.

EXPERIMENTAL PROCEDURES

Computational Details. PHASE 3.3 implemented in the Maestro 9.2 software package (Schrödinger, LLC) was used to derive the e-pharmacophore. Glide energy grids were generated for each of the prepared complexes. The binding site was defined by a rectangular box surrounding the ligand in the X-ray structure. Ligands were refined using the “Refine” option in Glide, and the Glide XP (extra precision) descriptor was chosen (Glide v5.7, Schrödinger, LLC, New York, NY). Default settings were used for the refinement and scoring.

Chemistry. All commercially available chemicals and solvents were used without further purification. TLC experiments were performed on alumina-backed silica gel 40 F254 plates (Merck, Darmstadt, Germany). The homogeneity of the compounds was monitored by thin layer chromatography (TLC) on silica gel 40 F254 coated on aluminum plates, visualized by UV light and KMnO₄ treatment. All ¹H and ¹³C NMR spectra were recorded on a Bruker AM-300 (300.12 MHz, 75.12 MHz) NMR spectrometer, BrukerBioSpin Corp., Germany. Molecular weights of the synthesized compounds were checked by LCMS 6100B series Agilent Technology. Chemical shifts are reported in ppm (δ) with reference to the internal standard TMS. The signals are designated as follows: s, singlet; d, doublet; dd, doublet of doublets; t, triplet; m, multiplet. Elemental analyses were carried out on an automatic Flash EA 1112 series, CHN Analyzer (Thermo). The purity of the final compounds was examined by HPLC (Shimadzu, Japan, (on Phenomenex C8 (150 mm × 4.6 mm, 5 μm, 100 Å) double

Table 3. Activities of Compounds 49–96



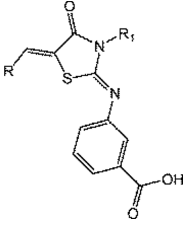
compd	R ₁	R ₂	R ₃	R ₄	R ₅	% inhibition at 500 nM	IC ₅₀ (nM)
49	methyl	bromo	H	H	H	50.5 ± 5.8	nd
50	ethyl	bromo	H	H	H	54.1 ± 9.9	nd
51	methyl	H	H	methoxy	H	88.6 ± 1.4	33.9 ± 3.6
52	ethyl	H	H	methoxy	H	56.2 ± 5.8	nd
53	methyl	H	H	chloro	H	59.7 ± 3.3	nd
54	ethyl	H	H	chloro	H	54.4 ± 15.2	nd
55	methyl	H	H	bromo	H	70.5 ± 3.7	nd
56	ethyl	H	H	bromo	H	60.9 ± 12.8	nd
57	methyl	H	H	benzyloxy	H	91.5 ± 2.2	25.6 ± 2.9
58	ethyl	H	H	benzyloxy	H	81.1 ± 3.1	nd
59	methyl	H	trifluoro-methyl	H	H	26.1 ± 10.9	nd
60	ethyl	H	trifluoro-methyl	H	H	26.0 ± 16.0	nd
61	methyl	chloro	H	H	H	54.6 ± 3.0	nd
62	ethyl	chloro	H	H	H	43.3 ± 11.6	nd
63	methyl	chloro	H	chloro	H	57.4 ± 7.6	nd
64	ethyl	chloro	H	chloro	H	45.4 ± 8.3	nd
65	methyl	benzyloxy	H	H	H	44.8 ± 5.9	nd
66	ethyl	benzyloxy	H	H	H	59.3 ± 0.8	nd
67	methyl	methoxy	H	H	H	96.9 ± 2.0	160.3 ± 20.3
68	ethyl	methoxy	H	H	H	59.5 ± 13.8	nd
69	methyl	H	H	isopropyl	H	54.0 ± 7.2	nd
70	ethyl	H	H	isopropyl	H	49.6 ± 8.7	nd
71	methyl	H	H	nitro	H	51.8 ± 10.2	nd
72	ethyl	H	H	nitro	H	32.7 ± 8.8	nd
73	methyl	H	H	H	H	52.2 ± 14.6	nd
74	ethyl	H	H	H	H	39.3 ± 9.4	nd
75	methyl	methyl	H	H	H	57.4 ± 14.6	nd
76	ethyl	methyl	H	H	H	47.0 ± 14.2	nd
77	methyl	H	methyl	H	H	49.6 ± 1.9	nd
78	ethyl	H	methyl	H	H	38.5 ± 6.7	nd
79	methyl	H	H	methyl	H	45.6 ± 9.6	nd
80	ethyl	H	H	methyl	H	41.7 ± 15.2	nd
81	methyl	H	methoxy	hydroxy	H	87.5 ± 2.1	60.0 ± 18.3
82	ethyl	H	methoxy	hydroxy	H	75.6 ± 0.7	nd
83	methyl	H	methoxy	methoxy	H	89.7 ± 1.0	54.3 ± 9.9
84	ethyl	H	methoxy	methoxy	H	90.9 ± 1.5	56.0 ± 4.4
85	methyl	H	H	trifluoromethyl	H	72.1 ± 8.1	nd
86	ethyl	H	H	trifluoromethyl	H	50.8 ± 6.5	nd
87	methyl	H	H	fluoro	H	89.5 ± 1.8	19.0 ± 1.1
88	ethyl	H	H	fluoro	H	68.3 ± 7.4	nd
89	methyl	H	chloro	chloro	H	60.0 ± 5.9	nd
90	ethyl	H	chloro	chloro	H	37.8 ± 14.5	nd
91	methyl	H	hydroxy	H	H	56.8 ± 5.6	nd
92	ethyl	H	hydroxy	H	H	52.8 ± 6.9	nd
93	methyl	H	H	N,N-dimethylamine	H	93.4 ± 2.4	37.0 ± 3.9
94	ethyl	H	H	N,N-dimethylamine	H	52.4 ± 7.8	nd
95	methyl	H	methoxy	methoxy	methoxy	89.4 ± 0.6	69.9 ± 1.2
96	ethyl	H	methoxy	methoxy	methoxy	37.4 ± 9.0	nd

end-capped RP-HPLC column)) and was >95%. Compounds 2–9 were commercially available and were purchased. The experimental details of the final, most potent analogues 18, 19, 22, 25, 28, 51, 57, 67, 81, 83, 84, 87, 93, and 95 are described below. A full description of

the synthetic protocol and spectroscopic analysis of all other compounds can be found in the Supporting Information.

General Procedure for the Synthesis of 18, 19, 22, 25, 28, 51, 57, 67, 81, 83, 84, 87, 93, and 95. To a well-stirred solution of

Table 4. Activities of Synthesized Compounds 97–106



compd	R ₁	R	% inhibition at 500 nM
97	methyl	furyl	30.1 ± 9.4
98	ethyl	furyl	29.2 ± 1.9
99	methyl	2-pyridyl	64.4 ± 4.5
100	ethyl	2-pyridyl	38.7 ± 11.4
101	methyl	2-pyrrole	58.4 ± 0.0
102	ethyl	2-pyrrole	32.5 ± 10.1
103	methyl	4-trifluoromethyl-3-pyridyl	34.4 ± 10.3
104	ethyl	4-trifluoromethyl-3-pyridyl	46.0 ± 10.9
105	methyl	3-indolyl	73.5 ± 6.5
106	ethyl	3-indolyl	61.9 ± 3.1

the 3-((3-alkyl-4-oxothiazolidin-2-ylidene)amino)benzoic acid (1 mmol) in ethanol (6 mL) was added dropwise piperidine (0.3 mmol) and the corresponding aldehyde (1.1 mmol). The reaction mixture was refluxed for 6 h (monitored by TLC and LCMS for completion) and evaporated to dryness. The residue was diluted with water (1 × 10 mL) and acidified with 2N HCl to pH 2. Dichloromethane (1 × 20 mL) was added to the reaction mixture, and the layers were separated. The aqueous layer was again extracted with dichloromethane (1 × 15 mL). The combined organic layer was washed with water (1 × 10 mL), brine (1 × 10 mL), dried over anhydrous sodium sulfate, and evaporated to dryness. The residue was then purified by column chromatography using hexane:ethyl acetate as eluent to give the desired product in good yield as described below.

3-((Z)-((Z)-5-(4-Hydroxybenzylidene)-3-methyl-4-oxothiazolidin-2-ylidene)amino)benzoic Acid (18). The compound was synthesized according to the general procedure using (Z)-3-((3-methyl-4-oxothiazolidin-2-ylidene)amino)benzoic acid (0.25 g, 1 mmol), piperidine (0.026 g, 0.3 mmol), and 4-hydroxybenzaldehyde (0.134 g, 1.1 mmol) to afford **18** as pale-yellow solid (0.22 g, 63%). ¹H NMR (DMSO-*d*₆): δ_H 3.33 (s, 3H), 6.82 (d, 2H, *J* = 8.5 Hz), 7.32–7.56 (m, 3H), 7.64–8.06 (m, 4H), 10.31 (br s, 1H). ¹³C NMR (DMSO-*d*₆): δ_C 167.1, 163.1, 160.1, 157.3, 148.6, 141.5, 131.3, 130.3, 129.7, 127.6, 127.1, 123, 115.8, 115.6, 30.2. EI-MS *m/z* (calcd for C₁₈H₁₄N₂O₄S, 354.38); found, 353.05 (M – H)[–]. Anal. Calcd for C₁₈H₁₄N₂O₄S: C, 61.01; H, 3.98; N, 7.90. Found: C, 60.03; H, 3.98; N, 7.88.

3-((Z)-((Z)-5-(4-Hydroxybenzylidene)-3-ethyl-4-oxothiazolidin-2-ylidene)amino)benzoic Acid (19). The compound was synthesized according to the general procedure using (Z)-3-((3-ethyl-4-oxothiazolidin-2-ylidene)amino)benzoic acid (0.25 g, 0.95 mmol), piperidine (0.024 g, 0.28 mmol), and 4-hydroxybenzaldehyde (0.127 g, 1.04 mmol) to afford **19** as off-white solid (0.25 g, 72%). ¹H NMR (DMSO-*d*₆): δ_H 1.26 (t, 3H, *J* = 7.11 Hz), 3.83 (q, 2H, *J* = 7.0 Hz), 6.84 (d, 2H, *J* = 8.5 Hz), 7.34–7.57 (m, 3H), 7.63–8.03 (m, 4H), 10.27 (br s, 1H). ¹³C NMR (DMSO-*d*₆): δ_C 166.5, 162.9, 160, 157.1, 148.4, 141.6, 131.2, 130.3, 129.6, 127.6, 122.8, 115.7, 115.4, 35.5, 12.1. EI-MS *m/z* (calcd for C₁₉H₁₆N₂O₄S, 368.41); found, 367.27 (M – H)[–]. Anal. Calcd for C₁₉H₁₆N₂O₄S: C, 61.94; H, 4.38; N, 7.60. Found: C, 61.92; H, 4.34; N, 7.62.

3-((Z)-((Z)-5-(4-Hydroxybenzylidene)-3-propyl-4-oxothiazolidin-2-ylidene)amino)benzoic Acid (22). The compound was synthesized according to the general procedure using (Z)-3-((3-propyl-4-oxothiazolidin-2-ylidene)amino)benzoic acid (0.25 g, 0.9 mmol), piperidine (0.023 g, 0.27 mmol), and 4-hydroxybenzaldehyde (0.121 g, 0.99 mmol) to afford **22** as pale-yellow solid (0.26 g, 76%). ¹H NMR (DMSO-*d*₆): δ_H 1.01 (t, 3H, *J* = 7.2 Hz), 1.76 (m, 2H), 3.89 (t, 1H, *J* = 7.5 Hz), 6.86 (d, 2H, *J* = 8.3 Hz), 7.36–7.56 (m, 3H), 7.65–

8.07 (m, 4H), 10.23 (br s, 1H). ¹³C NMR (DMSO-*d*₆): δ_C 166.3, 163, 159.8, 157.2, 148.4, 141.4, 131.1, 130.3, 129.4, 127.6, 126.8, 122.7, 115.7, 115.4, 43.5, 20, 11.2. EI-MS *m/z* (calcd for C₂₀H₁₈N₂O₄S, 382.43); found, 381.09 (M – H)[–]. Anal. Calcd for C₂₀H₁₈N₂O₄S: C, 62.81; H, 4.74; N, 7.33. Found: C, 62.80; H, 4.71; N, 7.34.

3-((Z)-((Z)-5-(4-Hydroxybenzylidene)-3-allyl-4-oxothiazolidin-2-ylidene)amino)benzoic Acid (25). The compound was synthesized according to the general procedure using (Z)-3-((3-allyl-4-oxothiazolidin-2-ylidene)amino)benzoic acid (0.25 g, 0.9 mmol), piperidine (0.023 g, 0.27 mmol), and 4-hydroxybenzaldehyde (0.122 g, 0.99 mmol) to afford **25** as buff-colored solid (0.23 g, 68%). ¹H NMR (DMSO-*d*₆): δ_H 4.51 (d, 2H, *J* = 5.3 Hz), 5.14–5.23 (m, 2H), 5.73–5.89 (m, 1H), 6.83 (d, 2H, *J* = 8.4 Hz), 7.34–7.58 (m, 3H), 7.68–8.06 (m, 4H), 10.35 (br s, 1H). ¹³C NMR (DMSO-*d*₆): δ_C 167, 163.2, 160.3, 157.3, 148.5, 141.3, 132.3, 131.2, 130.3, 129.6, 127.7, 127, 123, 117.1, 115.8, 115.5, 42.4. EI-MS *m/z* (calcd for C₂₀H₁₆N₂O₄S, 380.42); found, 379.06 (M – H)[–]. Anal. Calcd for C₂₀H₁₆N₂O₄S: C, 63.14; H, 4.24; N, 7.36. Found: C, 63.11; H, 4.26; N, 7.34.

3-((Z)-((Z)-5-(4-Hydroxybenzylidene)-3-isopropyl-4-oxothiazolidin-2-ylidene)amino)benzoic Acid (28). The compound was synthesized according to the general procedure using (Z)-3-((3-isopropyl-4-oxothiazolidin-2-ylidene)amino)benzoic acid (0.25 g, 0.9 mmol), piperidine (0.023 g, 0.27 mmol), and 4-hydroxybenzaldehyde (0.122 g, 0.99 mmol) to afford **28** as pale-yellow solid (0.28 g, 82%). ¹H NMR (DMSO-*d*₆): δ_H 1.47 (d, 6H, *J* = 7.01 Hz), 4.46 (sep, 1H, *J* = 7.02 Hz), 6.83 (d, 2H, *J* = 8.4 Hz), 7.33–7.57 (m, 3H), 7.64–8.04 (m, 4H), 10.18 (br s, 1H). ¹³C NMR (DMSO-*d*₆): δ_C 166.1, 162.6, 159.7, 156.9, 148.1, 141.3, 131, 130.4, 129.7, 127.5, 126.7, 122.4, 115.6, 115.3, 51.4, 20.1. EI-MS *m/z* (calcd for C₂₀H₁₈N₂O₄S, 382.43); found, 381.12 (M – H)[–]. Anal. Calcd for C₂₀H₁₈N₂O₄S: C, 62.81; H, 4.74; N, 7.33. Found: C, 62.79; H, 4.75; N, 7.33.

3-((Z)-((Z)-5-(4-Methoxybenzylidene)-3-methyl-4-oxothiazolidin-2-ylidene)amino)benzoic Acid (51). The title compound was synthesized according to the general procedure using (Z)-3-((3-methyl-4-oxothiazolidin-2-ylidene)amino)benzoic acid (0.25 g, 1 mmol), piperidine (0.026 g, 0.3 mmol), and 4-methoxybenzaldehyde (0.15 g, 1.1 mmol) to afford **51** as off-white solid (0.29 g, 78%). ¹H NMR (DMSO-*d*₆): δ_H 3.34 (s, 3H), 3.81 (s, 3H), 6.96 (d, 2H, *J* = 8.9 Hz), 7.34–8.07 (m, 7H). ¹³C NMR (DMSO-*d*₆): δ_C 166.6, 163.1, 160.3, 159.1, 148.2, 141.6, 131.2, 129.9, 129.6, 127.1, 126.9, 125.6, 122.9, 115.8, 113.8, 55.3, 30.2. EI-MS *m/z* (calcd for C₁₉H₁₆N₂O₄S, 368.41); found, 367.05 (M – H)[–]. Anal. Calcd for C₁₉H₁₆N₂O₄S: C, 61.94; H, 4.38; N, 7.60. Found: C, 61.95; H, 4.37; N, 7.60.

3-((Z)-((Z)-5-(4-Benzyloxy)benzylidene)-3-methyl-4-oxothiazolidin-2-ylidene)amino)benzoic Acid (57). The compound was synthesized according to the general procedure using (Z)-3-((3-methyl-4-oxothiazolidin-2-ylidene)amino)benzoic acid (0.25 g, 1 mmol), piperidine (0.026 g, 0.3 mmol), and 4-(benzyloxy)benzaldehyde (0.23 g, 1.1 mmol) to afford **57** as white solid (0.38 g, 86%). ¹H NMR (DMSO-*d*₆): δ_H 3.32 (s, 3H), 5.21 (s, 2H), 7.03–7.42 (m, 6H), 7.53–8.06 (m, 8H). ¹³C NMR (DMSO-*d*₆): δ_C 167, 163.2, 160.2, 157.8, 148.4, 141.6, 136.1, 131.1, 129.8, 129.5, 128.4, 127.1, 126.8, 126.4, 125.6, 122.7, 115.7, 113.6, 70.2, 30.4. EI-MS *m/z* (calcd for C₂₅H₂₀N₂O₄S, 444.50); found, 443.12 (M – H)[–]. Anal. Calcd for C₂₅H₂₀N₂O₄S: C, 67.55; H, 4.54; N, 6.30. Found: C, 67.52; H, 4.55; N, 6.29.

3-((Z)-((Z)-5-(2-Methoxybenzylidene)-3-methyl-4-oxothiazolidin-2-ylidene)amino)benzoic Acid (67). The compound was synthesized according to the general procedure using (Z)-3-((3-methyl-4-oxothiazolidin-2-ylidene)amino)benzoic acid (0.25 g, 1 mmol), piperidine (0.026 g, 0.3 mmol), and 2-methoxybenzaldehyde (0.15 g, 1.1 mmol) to afford **67** as off-white solid (0.29 g, 78%). ¹H NMR (DMSO-*d*₆): δ_H 3.35 (s, 3H), 3.83 (s, 3H), 6.98–7.03 (m, 2H), 7.23–7.31 (m, 2H), 7.64–8.08 (m, 5H). ¹³C NMR (DMSO-*d*₆): δ_C 167.1, 163.4, 160.1, 158.8, 148.3, 141.5, 131.1, 129.4, 128.5, 127.7, 126.8, 125.8, 122.8, 120.2, 115.7, 114.3, 113.6, 55.9, 30.5. EI-MS *m/z* (calcd for C₁₉H₁₆N₂O₄S, 368.41); found, 367.05 (M – H)[–]. Anal. Calcd for C₁₉H₁₆N₂O₄S: C, 61.94; H, 4.38; N, 7.60. Found: C, 61.97; H, 4.38; N, 7.62.

3-((Z)-((Z)-5-(4-Hydroxy-3-methoxybenzylidene)-3-methyl-4-oxothiazolidin-2-ylidene)amino)benzoic Acid (**81**). The compound was synthesized according to the general procedure using (Z)-3-((3-methyl-4-oxothiazolidin-2-ylidene)amino)benzoic acid (0.25 g, 1 mmol), piperidine (0.026 g, 0.3 mmol), and 4-hydroxy-3-methoxybenzaldehyde (0.17 g, 1.1 mmol) to afford **81** as pale-yellow solid (0.32 g, 84%). ¹H NMR (DMSO-*d*₆) δ_H 3.32 (s, 3H), 3.86 (s, 3H), 6.99–7.16 (m, 3H), 7.32–8.06 (m, 5H), 9.94 (br s, 1H). ¹³C NMR (DMSO-*d*₆): δ_C 166.8, 163.2, 160, 148.8, 148.6, 147.5, 141.6, 131.1, 129.6, 128.4, 127.1, 125.6, 123, 122.5, 116.4, 115.7, 111.5, 55.8, 30.4. EI-MS *m/z* (calcd for C₁₉H₁₆N₂O₅S, 384.41); found, 383.05 (M – H)[–]. Anal. Calcd for C₁₉H₁₆N₂O₅S: C, 59.37; H, 4.20; N, 7.29. Found: C, 59.35; H, 4.19; N, 7.29.

3-((Z)-((Z)-5-(3,4-Dimethoxybenzylidene)-3-methyl-4-oxothiazolidin-2-ylidene)amino)benzoic Acid (**83**). The compound was synthesized according to the general procedure using (Z)-3-((3-methyl-4-oxothiazolidin-2-ylidene)amino)benzoic acid (0.25 g, 1 mmol), piperidine (0.026 g, 0.3 mmol), and 3,4-dimethoxybenzaldehyde (0.18 g, 1.1 mmol) to afford **83** as light-brown solid (0.31 g, 78%). ¹H NMR (DMSO-*d*₆) δ_H 3.31 (s, 3H), 3.85 (s, 6H), 6.96–7.31 (m, 4H), 7.66–8.09 (m, 4H). ¹³C NMR (DMSO-*d*₆): δ_C 166.7, 163.2, 160.1, 149.4, 148.6, 148.4, 141.6, 131.1, 129.7, 128.1, 127, 125.6, 122.9, 122.1, 115.8, 111.3, 110.9, 55.7, 30.3. EI-MS *m/z* (calcd for C₂₀H₁₈N₂O₅S, 398.43); found, 397.06 (M – H)[–]. Anal. Calcd for C₂₀H₁₈N₂O₅S: C, 60.29; H, 4.55; N, 7.03. Found: C, 60.31 H, 4.54; N, 7.02.

3-((Z)-((Z)-5-(3,4-Dimethoxybenzylidene)-3-ethyl-4-oxothiazolidin-2-ylidene)amino)benzoic Acid (**84**). The compound was synthesized according to the general procedure using (Z)-3-((3-ethyl-4-oxothiazolidin-2-ylidene)amino)benzoic acid (0.25 g, 0.95 mmol), piperidine (0.024 g, 0.28 mmol), and 3,4-dimethoxybenzaldehyde (0.173 g, 1.04 mmol) to afford **84** as light-brown solid. ¹H NMR (DMSO-*d*₆) δ_H 1.24 (t, 3H, *J* = 7.05 Hz), 3.78 (q, 2H, *J* = 6.94 Hz), 3.84 (s, 3H), 3.86 (s, 3H), 6.94–7.31 (m, 3H), 7.61–8.05 (m, 5H). ¹³C NMR (DMSO-*d*₆): δ_C 166.2, 163.1, 159.8, 149.3, 148.5, 148.4, 141.7, 131, 129.6, 127.9, 126.8, 125.5, 123, 122, 115.9, 111.3, 110.8, 55.6, 35.4, 12.2. EI-MS *m/z* (calcd for C₂₁H₂₀N₂O₅S, 412.46); found, 411.11 (M – H)[–]. Anal. Calcd for C₂₁H₂₀N₂O₅S: C, 61.15; H, 4.89; N, 6.79. Found: C, 61.17; H, 4.87; N, 6.81.

3-((Z)-((Z)-5-(4-Fluorobenzylidene)-3-methyl-4-oxothiazolidin-2-ylidene)amino)benzoic Acid (**87**). The compound was synthesized according to the general procedure using (Z)-3-((3-methyl-4-oxothiazolidin-2-ylidene)amino)benzoic acid (0.25 g, 1 mmol), piperidine (0.026 g, 0.3 mmol), and 4-fluorobenzaldehyde (0.136 g, 1.1 mmol) to afford **87** as pale-yellow solid (0.33 g, 81%). ¹H NMR (DMSO-*d*₆): δ_H 3.31 (s, 3H), 7.20–7.34 (m, 3H), 7.68–8.08 (m, 6H). ¹³C NMR (DMSO-*d*₆): δ_C 166.8, 163, 161.7, 160.1, 148.3, 141.4, 131.1, 130.5, 130.1, 129.6, 127.1, 125.6, 123, 116.8, 115, 30.3. EI-MS *m/z* (calcd for C₁₈H₁₃FN₂O₃S, 356.37); found, 355.05 (M – H)[–]. Anal. Calcd for C₁₈H₁₃FN₂O₃S: C, 60.67; H, 3.68; N, 7.86. Found: C, 60.63; H, 3.70; N, 7.84.

3-((Z)-((Z)-5-(4-(Dimethylamino)benzylidene)-3-methyl-4-oxothiazolidin-2-ylidene)amino)benzoic Acid (**93**). The compound was synthesized according to the general procedure using (Z)-3-((3-methyl-4-oxothiazolidin-2-ylidene)amino)benzoic acid (0.25 g, 1 mmol), piperidine (0.026 g, 0.3 mmol), and 4-(dimethylamino)benzaldehyde (0.164 g, 1.1 mmol) to afford **93** as brownish-red solid (0.22 g, 58%). ¹H NMR (DMSO-*d*₆): δ_H 3.03 (s, 3H), 3.37 (s, 3H), 6.74 (d, 2H, *J* = 8.3 Hz), 7.34–7.47 (m, 3H), 7.66–8.12 (m, 4H). ¹³C NMR (DMSO-*d*₆): δ_C 166.6, 163.1, 160.2, 149.9, 148.5, 141.4, 131, 129.5, 129.3, 127.1, 125.6, 124.4, 122.9, 115.7, 111.4, 39.9, 30.3. EI-MS *m/z* (calcd for C₂₀H₁₉N₃O₃S, 381.45); found, 380.1 (M – H)[–]. Anal. Calcd for C₂₀H₁₉N₃O₃S: C, 62.97; H, 5.02; N, 11.02. Found: C, 62.95; H, 5.04; N, 11.03.

3-((Z)-((Z)-5-(3,4,5-Trimethoxybenzylidene)-3-methyl-4-oxothiazolidin-2-ylidene)amino)benzoic Acid (**95**). The compound was synthesized according to the general procedure using (Z)-3-((3-methyl-4-oxothiazolidin-2-ylidene)amino)benzoic acid (0.25 g, 1 mmol), piperidine (0.026 g, 0.3 mmol), and 3,4,5-trimethoxybenzaldehyde (0.22 g, 1.1 mmol) to afford **95** as off-white solid (0.36 g,

84%). ¹H NMR (DMSO-*d*₆): δ_H 3.37 (s, 3H), 3.83 (s, 3H), 3.87 (s, 3H), 6.81 (s, 2H), 7.32–8.13 (m, 5H). ¹³C NMR (DMSO-*d*₆): δ_C 166.9, 163.4, 160.3, 152.7, 148.6, 141.4, 138, 131.2, 129.6, 129, 127.1, 125.5, 123, 115.6, 103.4, 60.5, 55.8, 30.6. EI-MS *m/z* (calcd for C₂₁H₂₁N₃O₃S, 428.46); found, 427.11 (M – H)[–]. Anal. Calcd for C₂₁H₂₁N₃O₃S: C, 58.87; H, 4.70; N, 6.54. Found: C, 58.85; H, 4.68; N, 6.52.

CysK1 Hit Identification and Validation. Recombinant CysK1 was produced and purified as described previously.¹² Compounds were screened against *M. tuberculosis* CysK1 using an assay based on the spectrophotometric determination of the reaction product L-cysteine by ninhydrine³⁰ adapted to 96-well plate format described previously.¹² Each enzyme reaction was carried out at room temperature in a total volume of 50 μL containing 100 mM MOPS (pH 7.0), 2 mM *O*-acetyl-L-serine, 1 mM sodium sulfide, 5 pmol CysK1, and 2 mM, 500 μM, or 100 μM of the tested compounds. One μL of compound solution was transferred to all assay plates before 44 μL of reaction mix was added. The reactions were started by addition of 5 μL of sodium sulfide solution. After 20 min of incubation at 22 °C, the reactions were stopped by addition of 10 μL of trichloroacetic acid (final concentration, 16.6%). Subsequently, 60 μL of acid–ninhydrin reagent was added and the plates were heated at 96 °C for 10 min. Reactions were cooled and transferred into new 96-well plates, diluted 1:1 in ethanol (95%), and the absorbance of each sample was measured at 560 nm in a BioTek Synergy HT-1 plate reader. Each reaction was carried out in triplicate. Positive controls (100% inhibition) contained the assay mix with the inhibitory DFSI tetrapeptide (final concentration, 100 μM), negative controls (0% inhibition) did not contain any inhibitory compounds.

Compounds were designated as initial hits if the inhibition was >95%, and the IC₅₀ values for these were derived from dose–response curves. Serial 1:3 compound dilutions were first prepared in 50% dimethyl sulfoxide in 100 μL (final dimethyl sulfoxide concentration in assay: 5%) and transferred into a 96-deep well block. Then 890 μL of reaction mix was added (final concentrations: 100 mM MOPS [pH 7.0], 2 mM *O*-acetyl-L-serine, 1.25 μg CysK1) and the reactions started by addition of 10 μL of sodium sulfide (final concentration, 1 mM). The K_M for *O*-acetyl-L-serine is 5 mM and for Na₂S < 300 μM, hence the chosen substrate concentrations in the assay (2 mM OAS and 1 mM Na₂S) will favor identification of competitive inhibitors.³¹ This approach was validated by a Michaelis–Menten analysis of lead compound **2**, which indeed shows a competitive inhibition pattern (Supporting Information Figure S3). The K_i value of 111.2 nM for compound **2** also agrees well with the IC₅₀ value of 103.8 nM. At various time intervals (1, 2, 4, 6, 8, 10, 15, and 20 min), 100 μL aliquots were removed and assayed for L-cysteine formation as described above. This protocol ensures that the initial velocities are derived from the linear phase of the reaction. The initial rates were normalized to the initial rate for the CysK1-catalyzed reaction in the absence of inhibitors. The PI (percent inhibition) was calculated as 100% × (1 – normalized activity). The derived PI values were plotted against log[inhibitor concentration]. To determine the IC₅₀ values, a four-parameter nonlinear regression fit was performed with the program Origin (OriginLab) using equation: PI = Bottom + ((Top – Bottom)/(1 + 10^{((pXC₅₀ – log[hit compound]) × p)})), where bottom = minimal % inhibition, top = maximal % inhibition, *p* = Hill coefficient, and pXC₅₀ = –log(IC₅₀). As a positive control, the IC₅₀ value for the inhibitory peptide DFSI was determined under identical conditions. The resulting IC₅₀ for this peptide, 2.9 μM, compares well with the K_i of 5 μM determined previously.¹²

■ ASSOCIATED CONTENT

Supporting Information

Additional experimental details concerning e-pharmacophore modeling, library synthesis, docking, characterization of all synthesized compounds, spectroscopic data, and structural studies. This material is available free of charge via the Internet at <http://pubs.acs.org>.

Accession Codes

The PDB code for the structure of the complex of *M. tuberculosis* CysK1 with 2 is 3ZEL.

AUTHOR INFORMATION

Corresponding Author

*For D.S.: E-mail, drdsriram@yahoo.com. For G.S.: phone, +4652487675; fax, +468327626; E-mail, Gunter.Schneider@ki.se.

Author Contributions

[†]Ö.P. and V.U.J. contributed equally to this work.

Notes

The authors declare no competing financial interest.

ACKNOWLEDGMENTS

We gratefully acknowledge access to synchrotron radiation at the ESRF, France, BESSY, Germany, and MAX IV laboratory, Sweden. This work was supported by the Swedish Governmental Agency for Innovation Systems (VINNOVA) and the Department of Biotechnology (DBT), India.

ABBREVIATIONS USED

CysK1, O-acetylserine sulphydrylase; rt, room temperature

REFERENCES

- (1) Dye, C.; Williams, B. G. The Population Dynamics and Control of Tuberculosis. *Science* **2010**, *328*, 856–861.
- (2) Koul, A.; Arnoult, E.; Lounis, N.; Guillemont, J.; Andries, K. The challenge of new drug discovery for tuberculosis. *Nature* **2011**, *469*, 483–490.
- (3) Gengenbacher, M.; Kaufmann, S. H. E. *Mycobacterium tuberculosis*: success through dormancy. *FEMS Microbiol. Rev.* **2012**, *36*, 514–532.
- (4) Ehrt, S.; Schnappinger, D. Mycobacterial survival strategies in the phagosome: defence against host stresses. *Cell. Microbiol.* **2009**, *11*, 1170–1178.
- (5) Jothivasan, V. K.; Hamilton, C. J. Mycothiol: synthesis, biosynthesis and biological functions of the major low molecular weight thiol in actinomycetes. *Nat. Prod. Rep.* **2008**, *25*, 1091–1117.
- (6) Hampshire, T.; Soneji, S.; Bacon, J.; James, B. W.; Hinds, J.; Laing, K.; Stabler, R. A.; Marsh, P. D.; Butcher, P. D. Stationary phase gene expression of *Mycobacterium tuberculosis* following a progressive nutrient depletion: a model for persistent organisms. *Tuberculosis* **2004**, *84*, 228–238.
- (7) Betts, J. C.; Lukey, P. T.; Robb, L. C.; McAdam, R. A.; Duncan, K. Evaluation of a nutrient starvation model of *Mycobacterium tuberculosis* persistence by gene and protein expression profiling. *Mol. Microbiol.* **2002**, *43*, 717–731.
- (8) Voskuil, M. I.; Visconti, K. C.; Schoolnik, G. K. *Mycobacterium tuberculosis* gene expression during adaptation to stationary phase and low-oxygen dormancy. *Tuberculosis* **2004**, *84*, 218–227.
- (9) Schnappinger, D.; Ehrt, S.; Voskuil, M. I.; Liu, Y.; Mangan, J. A.; Monahan, I. M.; Dolganov, G.; Efron, B.; Butcher, P. D.; Nathan, C.; Schoolnik, G. K. Transcriptional adaptation of *Mycobacterium tuberculosis* within macrophages: Insights into the phagosomal environment. *J. Exp. Med.* **2003**, *198*, 693–704.
- (10) Bhawe, D. P.; Muse, W. B., III; Carroll, K. S. Drug targets in mycobacterial sulfur metabolism. *Infect. Disord. Drug Targets* **2007**, *7*, 140–158.
- (11) Hatzios, S. K.; Bertozzi, C. R. The Regulation of Sulfur Metabolism in *Mycobacterium tuberculosis*. *PLoS Pathogens* **2011**, *7*, e1002036 DOI: 10.1371/journal.ppat.1002036.
- (12) Schnell, R.; Oehlmann, W.; Singh, M.; Schneider, G. Structural insights into catalysis and inhibition of O-acetylserine sulphydrylase from *Mycobacterium tuberculosis*—crystal structures of the enzyme alpha-aminoacrylate intermediate and an enzyme–inhibitor complex. *J. Biol. Chem.* **2007**, *282*, 23473–23481.
- (13) Kumar, V. U. J.; Poyraz, O.; Saxena, S.; Schnell, R.; Yogeewari, P.; Schneider, G.; Sriram, D. Discovery of novel inhibitors targeting the *Mycobacterium tuberculosis* O-acetylserine sulphydrylase (CysK1) using virtual high-throughput screening. *Bioorg. Med. Chem. Lett.* **2013**, *23*, 1182–1186.
- (14) Friesner, R. A.; Murphy, R. B.; Repasky, M. P.; Frye, L. L.; Greenwood, J. R.; Halgren, T. A.; Sanschagrin, P. C.; Mainz, D. T. Extra Precision Glide: docking and scoring incorporating a model of hydrophobic enclosure for protein–ligand complexes. *J. Med. Chem.* **2006**, *49*, 6177–6196.
- (15) Friesner, R. A.; Banks, J. L.; Murphy, R. B.; Halgren, T. A.; Klicic, J. J.; Mainz, D. T.; Repasky, M. P.; Knoll, E. H.; Shelley, M.; Perry, J. K.; Shaw, D. E.; Francis, P.; Shenkin, P. S. Glide: a new approach for rapid, accurate docking and scoring. 1. Method and assessment of docking accuracy. *J. Med. Chem.* **2004**, *47*, 1739–1749.
- (16) Eldridge, M. D.; Murray, C. W.; Auton, T. R.; Paolini, G. V.; Mee, R. P. Empirical scoring functions: I. The development of a fast empirical scoring function to estimate the binding affinity of ligands in receptor complexes. *J. Comput.-Aided. Mol. Des.* **1997**, *11*, 425–445.
- (17) Dayam, R.; Aiello, F.; Deng, J.; Wu, Y.; Garofalo, A.; Chen, X.; Neamati, N. Discovery of Small Molecule Integrin $\alpha V\beta 3$ Antagonists as Novel Anticancer Agents. *J. Med. Chem.* **2006**, *49*, 4526–4534.
- (18) Vicini, P.; Geronikaki, A.; Incerti, M.; Zani, F.; Dearden, J.; Hewitt, M. 2-Heteroarylrimino-5-benzylidene-4-thiazolidinones analogues of 2-thiazolylimino-5-benzylidene-4-thiazolidinones with antimicrobial activity: synthesis and structure–activity relationship. *Bioorg. Med. Chem.* **2008**, *16*, 3714–3724.
- (19) Verma, A.; Saraf, K. S. 4-Thiazolidinone A biologically active scaffold. *Eur. J. Med. Chem.* **2008**, *43*, 897–905.
- (20) Jain, K. A.; Vaidya, A.; Ravichandran, V.; Kashaw, S. K.; Agrawal, K. R. Recent developments and biological activities of thiazolidinone derivatives: A review. *Bioorg. Med. Chem.* **2012**, *20*, 3378–3395.
- (21) Maccari, R.; Ottana, R.; Curinga, C.; Vigorita, M. G.; Rakowitz, D.; Steindlb, T.; Langer, T. Structure–activity relationships and molecular modelling of 5-aryliden-2,4-thiazolidinediones active as aldose reductase inhibitors. *Bioorg. Med. Chem.* **2005**, *13*, 2809–2823.
- (22) Kosma, P.; Selzer, E.; Mereiter, K. 4-[(Z)-5-[(Z)-3-Ethoxy-4-hydroxybenzylidene]-3-methyl-4-oxo-1,3-thiazolidin-2-ylidene}-amino]benzoic acid dimethylformamide monosolvate. *Acta Crystallogr., Sect. E: Struct. Rep. Online* **2012**, *E68*, o3417–o3418.
- (23) Huang, B.; Vetting, M. W.; Roderick, S. L. The active site of O-acetylserine sulphydrylase is the anchor point for bienzyme complex formation with serine acetyltransferase. *J. Bacteriol.* **2005**, *187*, 3201–3205.
- (24) Francois, J. A.; Kumaran, S.; Jez, J. M. Structural basis for interaction of O-acetylserine sulphydrylase and serine acetyltransferase in the Arabidopsis cysteine synthase complex. *Plant Cell* **2006**, *18*, 3647–3655.
- (25) Salsi, E.; Bayden, A. S.; Spyarakis, F.; Amadasi, A.; Campanini, B.; Bettati, S.; Dodato, T.; Cozzini, P.; Kellogg, G. E.; Cook, P. F.; Roderick, S. L.; Mozzarelli, A. Design of O-acetylserine sulphydrylase inhibitors by mimicking nature. *J. Med. Chem.* **2010**, *53*, 345–356.
- (26) Campanini, B.; Speroni, F.; Salsi, E.; Cook, P. F.; Roderick, S. L.; Huang, B.; Bettati, S.; Mozzarelli, A. Interaction of serine acetyltransferase with O-acetylserine sulphydrylase active site: evidence from fluorescence spectroscopy. *Protein Sci.* **2005**, *14*, 2115–2124.
- (27) Spyarakis, F.; Felici, P.; Bayden, A. S.; Salsi, E.; Miggiano, R.; Kellogg, G. E.; Cozzini, P.; Cook, P. F.; Mozzarelli, A.; Campanini, B. Fine tuning of the active site modulates specificity in the interaction of O-acetylserine sulphydrylase isozymes with serine acetyltransferase. *Biochim. Biophys. Acta* **2013**, *1834*, 169–181.
- (28) Nagpal, I.; Raj, I.; Subbarao, N.; Gourinath, S. Virtual screening, identification and in vitro testing of novel inhibitors of O-acetyl-L-serine sulphydrylase of *Entamoeba histolytica*. *PLoS One* **2012**, *7*, e30305 DOI: 10.1371/journal.pone.0030305.
- (29) Amori, L.; Katkevica, S.; Bruno, A.; Campanini, B.; Fekici, P.; Moxxearelli, A.; Costantino, G. Design and synthesis of trans-2-

substituted-cyclopropane-1-carboxylic acids as the first non-natural small molecule inhibitors of O-acetylserine sulphydrylase. *Med. Chem. Commun.* **2012**, 3, 1111–1116.

(30) Gaitonde, M. K. A spectrophotometric method for the direct determination of cysteine in the presence of other naturally occurring amino acids. *Biochem. J.* **1967**, 104, 627–633.

(31) Wu, G.; Yuan, Y.; Hodge, C. N. Determining appropriate substrate conversion for enzymatic assays in high-throughput screening. *J. Biomol. Screening* **2003**, 8, 694–700.